Solar-Terrestrial Physics. 2025. Vol. 11. Iss.1. P. 49–55. DOI: 10.12737/stp-111202506. © 2025 A.A. Karakhanyan, S.I. Molodykh. Published by INFRA-M Academic Publishing House

DOI: 10.12737/stp-111202506

Received July 05, 2024
Accepted November 20, 2024

TROPOSPHERIC RESPONSE TO SOLAR EFFECTS DURING GEOMAGNETIC SUPERSTORMS IN SOLAR CYCLE 23

A.A. Karakhanyan
Institute of Solar-Terrestrial Physics SB RAS, Irkutsk, Russia, asha@iszf.irk.ru

S.I. Molodykh
Institute of Solar-Terrestrial Physics SB RAS, Irkutsk, Russia, sim@iszf.irk.ru

Abstract. The ionospheric electric potential (*EP*) is used as a heliogeophysical parameter to analyze tropospheric response to solar impacts during geomagnetic superstorms in solar cycle 23. According to observational data, the response of meteoparameters is shown to concur with *EP* variations during the November 20, 2003 geomagnetic superstorm caused by an extreme geoeffective event. The tropospheric response is time-shifted versus *EP* maximum during the July 15, 2000 magnetic superstorm: increased precipitable water is observed in 6 hrs; decreased outgoing longwave radiation, in 12 hrs; increased upper cloudiness, in 18 hrs. We have found that the amplitude of the meteoparameters' response to *EP* variations during the July 15, 2000 magnetic superstorm is about half as low as that of the tropospheric response during the November 20, 2003 geomagnetic superstorm.

Keywords: ionospheric electric potential, solar activity, geomagnetic index, outgoing longwave radiation, cloudiness, water vapor, climate.

INTRODUCTION

The electric potential (*EP*) of the ionosphere can be used as one of the heliogeophysical parameters for analyzing processes in the magnetosphere—ionosphere—troposphere system. The most well-known electric mechanisms of the effect of solar activity on the troposphere involve determining changes in incoming solar radiation. The ionospheric electric field through changes in the global electric circuit alters microphysics of clouds and hence the incoming short-wave radiation [Tinsley, 2000; Kniveton et al., 2008; Harrison, Lockwood, 2020]. According to the electric mechanism developed at ISTP SB RAS, variations in solar activity through changes in solar wind (SW) and interplanetary magnetic field (IMF) parameters affect the magnetospheric convection, which, in turn, has an effect on the distribution of the *EP* difference between the ionosphere and the earth. An increase in *EP* leads to a restructuring of the vertical profile of the volume electric charge, which affects the phase state of water vapor (cloud formation in the atmosphere increases), and to a change in the cluster composition in cloudless regions (the number of dimers and larger clusters increases). Accordingly, optical properties of water vapor change in the infrared spectrum, thereby enhancing the atmospheric greenhouse effect. This causes the radiation balance, in particular the outgoing longwave radiation (λ>4 μm), to change [Molodykh et al., 2020]. All characteristics of solar/geomagnetic activity have been developed to describe dynamic processes on the Sun and in near-Earth space. Studying climatic changes associated with solar exposure assumes the presence of a characteristic reflecting the solar impact that reaches Earth and has a long range. The relative number of sunspots (Wolf number) is most often used in the problem of solar-tropospheric relations [Ishkov, 2018]. A long sequence of Wolf numbers is employed to study cyclicity in long-term variations of meteorological parameters. Geomagnetic indices correspond better to a given condition, but they describe, first of all, geomagnetic variations lasting less than three hours, and their globality does not allow us to create distribution in space [Gavrilov et al., 2016; Yamazaki et. al., 2022]. We have previously explored the possibility of utilizing *EP* as an indicator of solar effects on the troposphere. In [Karakhanyan, Molodykh, 2023], we have analyzed the space-time dynamics of *EP* variations in current warming, using satellite data on the SW magnetic field and plasma parameters in near-Earth space. The trend for *EP* to rise has been observed for the past three solar cycles. The opposite trend is typical of geomagnetic indices. The discovered synchronicity of long-term variations in *EP* and near-surface temperature is likely to depend on the large-scale magnetic field of the Sun to a greater extent than on the small-scale one, and affects parameters of the climate system. Solar cycle 23 is a transition period between the epochs of increased and decreased solar activity (SA). It is a medium cycle and the second component of the physical 22-year cycle of changing the polarity of magnetic poles in the maximum phase of the 11-year cycle. The most powerful flare events occurred not only at the maximum, but also in the descending phase of the cycle. Let us mention some features of its development: characteristic signs of stable (non-flare) active regions, prolonged high flare activity in the descending phase of the cycle, an increase in the number of quiet geomagnetic days due to a decrease in flare activity. These features suggest that the mode of magnetic field generation in the

convective zone of the Sun changes. In this case, the Sun enters a period of medium and short cycles, which can last from 50 to 100 years [Ishkov, 2005; Ishkov, 2018]. The purpose of this work is to analyze the response of meteorological parameters (outgoing longwave radiation, precipitable water, upper cloudiness) to *EP* variations during individual geomagnetic superstorms in solar cycle 23.

1. DATA AND ANALYSIS METHOD ANALYSIS

The most geoeffective flares during maximum of solar cycle 23 are associated with the passage of a large sunspot group of AR9077 in the second decade of July 2000. The magnetic superstorm on July 15, 2000 was caused by one of the largest solar flares on record called "Bastille Day flare" (see Table 1). Intense flare activity in the cycle was observed in October–November 2003. A complex event on November 18 led to an extreme geoeffective impact on near-Earth space. The geomagnetic storm recorded on November 20, 2003 is the most powerful in the cycle with *Dst*=–422 nT [Ishkov, 2005; Grechnev et al., 2014; https://wdc.kugi.kyoto-u.ac.jp/wdc/Sec3.html].

Spatial distribution of *EP* was computed using the code of the 2000 Weimer model written in IDL. In this version of the semi-empirical Weimer model, the horizontal structure of the electric field is determined by variations in the SW, IMF parameters and by the geomagnetic activity index *AL*. The last parameter is included to account for the effect of nighttime magnetospheric substorms on the *EP* structure [Weimer, 2001]. Events on a time scale from hours to several days are analyzed assuming that regular variations in electric potential and other parameters change little. The tropospheric response is studied for latitudes above 60° N, therefore we took the geomagnetic index *AE*, which describes geomagnetic disturbances at high latitudes. Hourly-resolved data on the interplanetary medium and the geomagnetic indices (*AE*, *AL*) have been taken from the OMNI database [https://omniweb.gsfc.nasa.gov/html/ow_data.html]. We have used hourly meteorological parameters from the CERES-SYN1deg dataset in the 1.0°×1.0° grid [Wielicki et al., 1996, CERES_ SYN1deg Ed4.1SubsettingandBrowsing]. Outgoing longwave radiation (*OLR*) is represented by the broadband emitted thermal outgoing flux observed by CERES in the upper atmosphere (*h*~20 km). The Cloud Area Fraction is the fraction of the sky covered by high-level clouds (from 300 hPa to the tropopause) and expressed as a percentage. Precipitable water is the total mass of water vapor in the vertical air column (from the surface to *h*), expressed by the height of the layer *W* of the equivalent mass of accumulated precipitated water if it were condensed. In the troposphere, there is a natural synoptic period (*NSP*) — a period of time during which cyclones/anticyclones continue to move and the location of their centers is the same in a certain region or throughout the hemisphere (*NSP* ~ 7 days). To minimize the influence of synoptic processes, we calculated the anomalies of the analyzed parameters relative to daily average variations 7 days before the event and analyzed the dynamics of anomalies of the characteristics considered, averaged for latitudes above 60° N, during selected magnetic storms. The *EP* anomaly maps were calculated from the formula

$$\Delta EP_{ij} = EP_{ij} - \frac{1}{n}\sum_{k=-7}^{k=-1} EP_{kj},$$

where *i* is the number of disturbed day; *j* is the number of hour in the day; *k* is the number of day for calculating daily average variations; *n*=7. Maps of anomalies of meteorological parameters are computed in a similar way.

Table 1

Heliogeophysical conditions during magnetic supestorms in SC 23

Event date	Solar flare characteristics				Date and *Dst*, nT
	date	class	Active region	heliocoordinates	
Jul. 15–16, 2000	Jul. 14, 2000	X5.7/3B	9077	22° N 07° W	Jul. 16, 2000, *Dst*=–301 nT
Nov. 20–21, 2003	Nov. 18, 2003	M3.2	10501	00° N 18° E	Nov. 20, 2003, *Dst*=–422 nT

Table 2

Input IMF and SW parameters for calculating *EP* anomalies by the Weimer model

Hour	B_y, nT	B_z, nT	*V*, km/s	*n*, cm^{-3}	|*B*|	angle, deg.	*AL*, nT
Quiet conditions on November 18, 2003							
17 UT	–0.6	–1.8	683	2.4	1.9	198.4	–372
Disturbed conditions on November 20, 2003							
16 UT	12.9	–50.1	584	16.1	51.73	165.6	–1790
17 UT	–2.2	–44.4	596	18.7	44.45	182.8	–1619
18 UT	–12.0	–37.5	580	18.7	39.37	197.7	–1030
Quiet conditions on July13, 2000							
20 UT	4.0	–0.6	607	4.6	4.0	98.5	–110
Disturbed conditions on July 15, 2000							
19 UT	13.2	–35.3	1000	20.6	37.7	159.5	–797
20 UT	17.6	–45.3	1040	5.9	48.6	158.8	–1088
21 UT	38.7	–19.9	1107	7.2	43.5	117.2	–620

2. RESULTS

Magnetic superstorms of solar cycle 23 featured extreme values of parameters on the Sun, in Earth's magnetosphere and ionosphere [Ermolaev et al., 2005; Blagoveshchenskaya et al., 2005; Kleimenova, Kozyreva, 2009; Kim et al., 2011]. The dynamics of variations in *EP*, *AE*, and the meteorological parameters averaged for the latitude region above 60° N is shown in Figure 1. The sudden commencement of the magnetic storm on November 20, 2003 was detected at 08 UT; its main phase, according to *Dst*, began at 12 UT. Analysis has revealed that *EP* variations anticorrelate with *AE* in the initial phase of the storm (r=–0.80±0.35). Correlation between the parameters considered is observed from 18 UT during the storm main phase to 09 UT on November 21 during the recovery phase (r=0.83±0.15). The tropospheric response occurs simultaneously with *EP* variations from 08 UT to 18 UT on November 21: *W* increases (r=0.75±0.12), *OLR* decreases (r=–0.53±0.15), upper cloudiness increases (r=0.19±0.17). *W* peaks 1 hr after the *EP* maximum. The maximum response of *OLR* to *EP* variations occurs 3 hrs after the *EP* maximum. Maximum upper cloudiness is observed later than the response of precipitable water and *OLR* to *EP* variations. Upper cloudiness peaks within 6 hrs after the *EP* maximum. Another decrease in *OLR* is recorded after the maximum increase in cloudiness, i.e. it might have resulted from an increase in upper cloudiness (see Figure 1, top left panel).

Peculiarities in the behavior of the *EP* and *AE* variations in general persist during the July 15, 2000 magnetic superstorm, which began at 14:37 UT. The *EP* variations correlate with *AE* in the storm initial phase at 15–18 UT (r=–0.56±0.59). The analyzed parameters correlate from 20 UT during the main phase to the end of the early recovery phase (09 UT on July 16, r=0.93±0.11). The maximum response of the meteorological parameters to *EP* variations shifts in time relative to its maximum: *W* increases within 6 hrs, *OLR* decreases within 12 hrs, high-level clouds increase within 18 hrs. Note that the amplitude of the tropospheric response to *EP* variations during the July 15, 2000 magnetic storm is approximately twice as low as that of the response of meteorological parameters during the November 20, 2003 geomagnetic storm (see Figure 1, top right panel).

The spatial distribution of isopotentials, illustrated in Figures 2, 3, was calculated for the interplanetary medium conditions according to Table 2: B_y and B_z are IMF components; *V* is the SW velocity; *n* is the proton density; the IMF angle is –180°÷180°; 0 is the north; *AL* is a geomagnetic activity index.

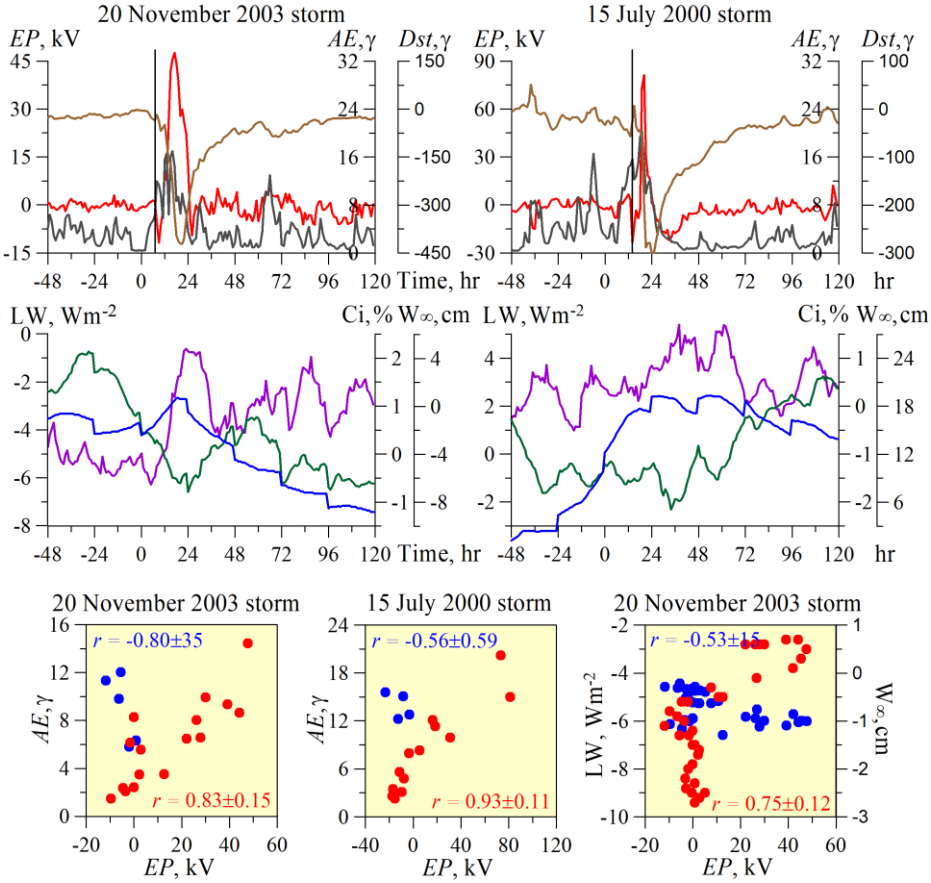

Figure 1. Changes in *EP* anomalies (red line), meteorological parameters and geomagnetic indices (top and middle panels): $AE\times10^2$ (black); *OLR* (green); high-level clouds (Ci) (purple); precipitable water ($W_\infty\times10^{-2}$) (blue). Meteorological parameters are averaged for a latitude region above 60° N over a 7 day interval during geomagnetic superstorms. The vertical line indicates the onset of the geomagnetic storm. Zero on the horizontal axis is 00 UT of the day of the geomagnetic storm onset. Scatter plots of hourly *EP* and *AE*, *EP* and meteorological parameters (bottom panel)

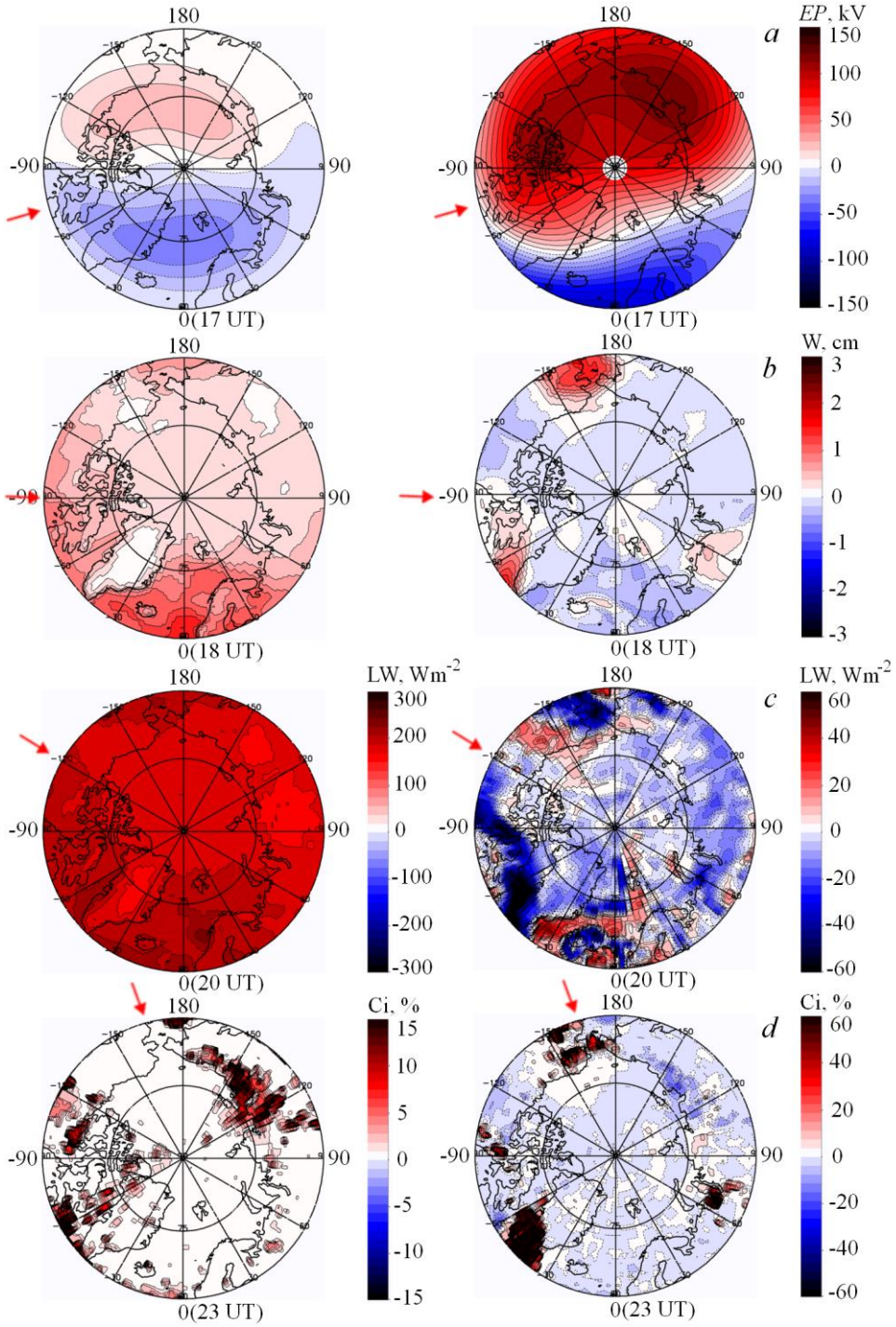

Figure 2. Spatial distribution of *EP* anomalies (*a*), precipitable water (*b*), *OLR* (*c*), upper cloudiness (*d*) during a quiet period (left) and at their maximum (right) during the November 20, 2003 geomagnetic superstorm for a latitude region above 60° N. The midday meridian is shown by arrows, with the maximum time of the event in parentheses

Figure 2 exhibits the structure of the analyzed parameters in space for a quiet period and the spatial structure of their maximum response to the November 20, 2003 event. We have found that an increase in *EP* during the disturbance occurs with an increase in *W*, a decrease in *OLR*, and a less pronounced increase in upper cloudiness. A similar tropospheric response to *EP* variations was observed during the July 15, 2000 geomagnetic storm. Yet, its spatial structure is less pronounced due to changes in meteorological parameters in the annual variation with corresponding seasonal variations, in atmospheric circulation, which in summer exhibits instability of the troposphere caused by the development of cyclonic activity in the hemisphere (Figure 3). The features found in the behavior of the tropospheric response to *EP* variations are consistent with the theoretical mechanism of the solar activity effect on the climate system, developed at ISTP SB RAS. The mechanism suggests that a determining factor in estimating the magnitude of the tropospheric response during disturbances is a change in optical properties of water vapor in the troposphere.

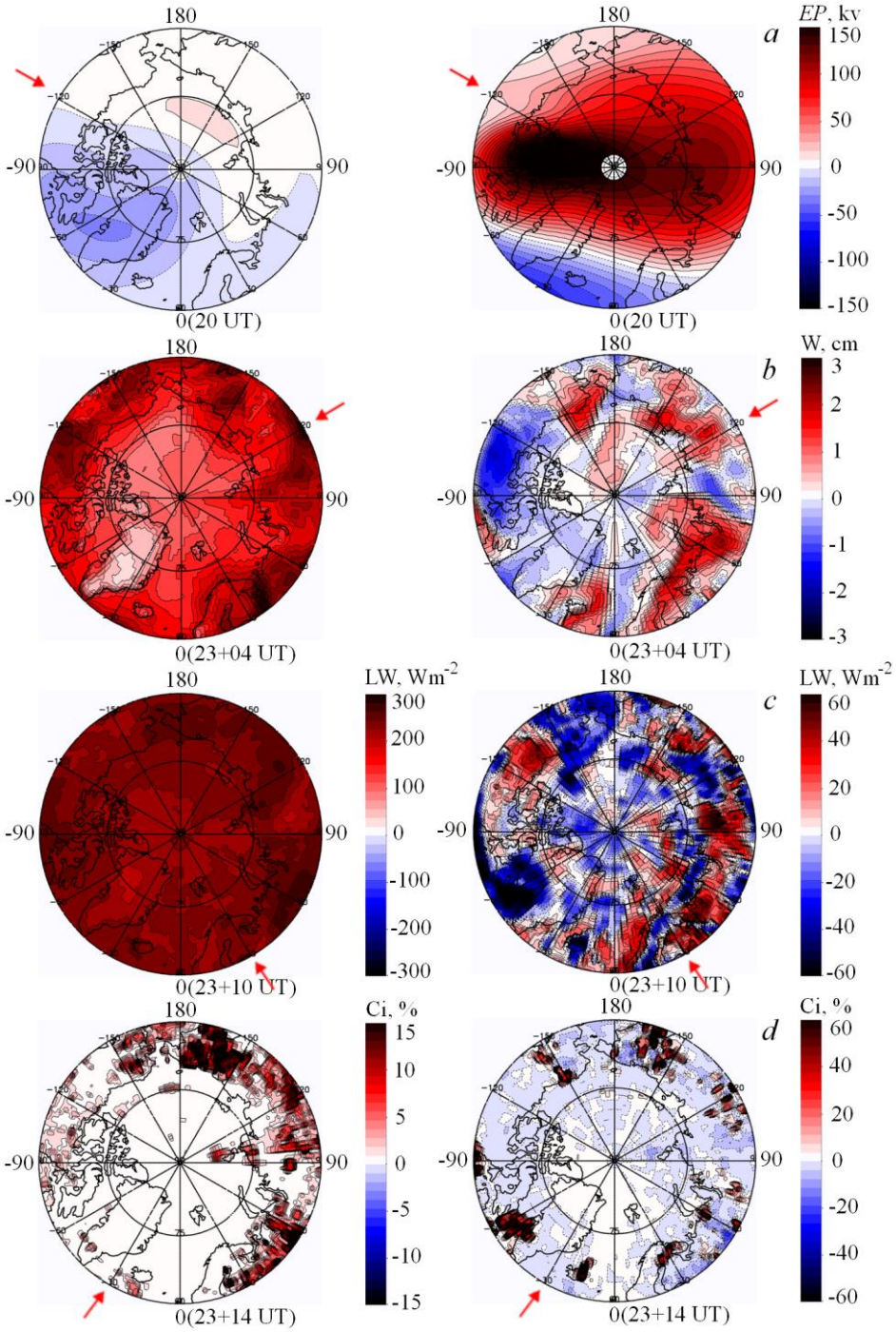

Figure 3. The same as in Figure 2 for the July 15, 2000 storm

3. DISCUSSION

Addressing the problem of the effect of solar processes on the climate system allowed us to define *EP* as an optimal proxy of solar activity. The detected anticorrelation between *EP* and *AE* variations during the events confirms the assumption that *EP* variations reflect both sporadic processes and slow changes in the general magnetic field of the Sun, unlike the indices that measure the degree of geomagnetic disturbance. From satellite data, we have found that an increase in *EP* is accompanied by an increase in *W*, a decrease in *OLR*, and an increase in high-level clouds in the high-latitude troposphere during geomagnetic superstorms of SC 23. The spatial structure of the tropospheric response to solar influence is known to depend on both the power of events and tropospheric conditions. According to the results obtained in [Grechnev et al., 2014], the analyzed events are similar in the location of sources near the center of the solar disk and the intensity of the geomagnetic effect, which was determined by the parameters of the solar sources such as very strong IMF>50 nT and a large southward B_z component. The extreme geomagnetic effect on November 20, 2003 was clearly manifested in the winter atmosphere.

The minimum delay in the response of the meteorological parameters to the increase in *EP* was hours and was observed during the November 20, 2003 geomagnetic superstorm. The results are well described by the physical mechanism, developed at ISTP SB RAS, in which solar activity affects the ability of water vapor (the main greenhouse gas) to absorb in the infrared band [Molodykh et al., 2020]. Search for a solar signal in climatic changes by studying the dynamics of outgoing radiation during events differentiates our hypothesis from other mechanisms of solar activity influence on climate, which involve studying changes in incoming radiation. Note that the use of *EP* as a heliogeophysical parameter allow us to reduce the disadvantages characteristic of the geomagnetic indices, but the limitation associated with nonlinearity of the solar-troposphere relation persists on a time scale <3 hrs. According to our mechanism, solar activity may be one of the factors affecting the formation of cloud radiative forcing (*CRF*). The results obtained from ERBE data suggest that global mean *CRF*=–15 W/m^2 [Kondratyev, Krapivin, 2006]. Model calculations have shown that the negative shortwave effect (cooling) is greater than the positive longwave effect (heating) of cloudiness on the underlying surface — atmosphere system [Kondratyev, 1992]. In follow-up studies, it is planned to include *EP* as a proxy of solar activity in parameterization of cloud formation for the model block of radiation transfer in the atmosphere. Comparison between results of numerical simulation and observations will allow us to assess the contribution of solar activity to changes in Earth radiation balance components.

CONCLUSIONS

The analysis of the tropospheric response to *EP* variations during severe geomagnetic storms in SC 23 has allowed us to formulate the following results.

1. The positive relationship between *EP* and *AE* variations breaks down during the main phase of severe geomagnetic storms. The detected feature suggests that *EP* variations reflect both sporadic processes and slow changes in the large-scale magnetic field of the Sun, unlike the geomagnetic indices that measure the degree of geomagnetic disturbance.

2. The response of meteorological parameters occurs simultaneously with *EP* variations during the November 20, 2003 magnetic superstorm, caused by an extremely geoeffective event.

3. The tropospheric response shifts in time relative to the maximum of *EP* during the July 15, 2000 magnetic superstorm: *W* increases in 6 hrs, *OLR* decreases in 12 hrs, high-level clouds increase in 18 hrs.

4. The amplitude of the response of meteorological parameters to *EP* variations during the July 15, 2000 magnetic storm is approximately half as low as that of the tropospheric response during the November 20, 2003 geomagnetic storm.

We thank Prof. D.R. Weimer for providing the model code for calculating *EP*. We express our gratitude to the reviewer for carefully reading the manuscript and valuable comments that contribute to its improvement.

The work was financially supported by the Ministry of Science and Higher Education of the Russian Federation.

REFERENCES

Blagoveshchenskaya N.F., Kornienko V.A., Borisova T.D., Moskvin I.V., Berdnikova M.Yu., Yanzhura A.S., Blagoveshchenskii D.V. Ionospheric effects during the main phase of the magnetic storm of November 20, 2003, in the European Arctic regions. *Geomagnetizm i aeronomiya* [Geomagnetism and Aeronomy]. 2005, vol. 45, iss. 1, pp. 60–70. (In Russian).

Ermolaev Yu.I., Zelenyi L.M., Zastenker G.N., Petrukovich A.A., Mitrofanov I.G., Litvak M.L., et al. Solar and heliospheric disturbances that resulted in the strongest magnetic storm of November 20, 2003. *Geomagnetizm i aeronomiya* [Geomagnetism and Aeronomy]. 2005, vol. 45, iss. 1, pp. 23–46. (In Russian).

Gavrilov B.G., Ryakhovskiy I.A., Markovich I.E., Lyakhov A.N., Egorov D.V. The applicability of the station and the planetary geomagnetic activity indices. *Geliogeofizicheskie issledovaniya* [Heliogeophys. Res.]. 2016, no. 15, pp. 42–48. (In Russian).

Grechnev V.V., Uralov A.M., Chertok I.M., Belov A.V., Filippov B.P., Slemzin V.A., Jackson B.V. A challenging solar eruptive event of 18 November 2003 and the causes of the 20 November geomagnetic superstorm. IV. Unusual magnetic cloud and overall scenario. *Solar Phys.* 2014, vol. 289, iss. 12, pp. 4653–4673. DOI: 10.1007/s11207-014-0596-5.

Harrison R.G., Lockwood M. Rapid indirect solar responses observed in the lower atmosphere. *Proc. the Royal Society A.* 2020, vol. 476, iss. 2241, p. 20200164.DOI: 10.1098/rspa.2020.0164.

Ishkov V.N. Properties of the current 23rd solar-activity cycle. *Solar System Research.* 2005, vol. 39, iss. 6, pp. 453–461.

Ishkov V.N. Space weather and specific features of the development of current solar cycle. *Geomagnetizm i aeronomiya* [Geomagnetism and Aeronomy]. 2018, vol. 58, iss. 6, pp. 753–767. DOI: 10.1134/S0016793218060051. (In Russian).

Karakhanyan A.A., Molodykh S.I. Ionospheric electric potential as an alternative indicator of solar effect on the lower atmosphere. *Solar-Terrestrial Physics*. 2023, vol. 9, iss. 2, pp. 103–106. DOI: 10.12737/stp-92202313.

Kim V.P., Hegal V.V., Min K.W., Lee J.J. Regional morphology features of electron concentration disturbances at the mid-latitude F2-layer maximum during magnetic superstorm of July 15, 2000. *Geomagnetizm i aeronomiya* [Geomagnetism and Aeronomy]. 2011, vol. 51, iss. 2, pp. 254–266. DOI: 10.1134/ S0016793211020083. (In Russian).

Kleimenova N.G., Kozyreva O.V. The recovery phase of the superstrong magnetic storm of July 15–17, 2000: substorms and ULF pulsations. *Geomagnetizm i aeronomiya* [Geomagnetism and Aeronomy]. 2009, vol. 49, iss. 3, pp. 60–70. DOI: 10.1134/S0016793209030049. (In Russian).

Kniveton D.R., Tinsley B.A., Burns G.B., Bering E.A., Troshichev O.A. Variations in global cloud cover and the fair-weather vertical electric field. *J. Atmos. Solar-Terr. Phys.* 2008, vol. 70, iss. 13, pp. 1633–1642. DOI: 10.1016/j.jastp.2008.07.001.

Kondratyev K.Ya. The global climate. SPb.: Nauka, St. Petersburg branch, 1992, 359 p.

Kondratyev K.Ya., Krapivin V.F. Earth's radiation budget as an indicator of the global ecological equilibrium. *Issledovanie Zemli iz kosmosa* [Research of the Earth from Space]. 2006, no. 1, pp. 3–9. (In Russian).

Molodykh S.I., Zherebtsov G.A., Karakhanyan A.A. Estimation of solar activity impact on the outgoing infrared-radiation flux. *Geomagnetizm i aeronomiya* [Geomagnetism and Aeronomy]. 2020, vol. 60, iss. 2, pp. 205–211. DOI: 10.1134/S0016793220020103. (In Russian).

Tinsley B.A. Influence of solar wind on the global electric circuit, and inferred effects on cloud microphysics, temperature, and dynamics in the troposphere. *Space Sci. Rev.* 2000, vol. 94, iss. 1-2, pp. 231–258.

Weimer D.R. An improved model of ionospheric electric potentials including substorm perturbations and application to the Geospace Environment Modeling November 24, 1996, event. *J. Geophys. Res.: Space Phys.* 2001, vol. 106, iss. A1, pp. 407–416.

Wielicki B.A., Barkstrom B.R., Harrison E.F., Lee III R.B., Smith G.L., Cooper, J.E. Clouds and the Earth's Radiant Energy System (CERES): An Earth Observing System Experiment. *Bulletin of the American Meteorological Society*. 1996, vol. 77, iss. 5, pp. 853–868.

Yamazaki Y., Matzka J., Stolle C., Kervalishvili G., Rauberg J., Bronkalla O., et al. Geomagnetic activity index Hpo. *Geophys. Res. Lett.* 2022, vol. 49, iss. 10, e2022GL098860. DOI: 10.1029/2022GL098860.

URL: CERES_SYN1degEd4.1SubsettingandBrowsing (accessed July 5, 2024).

URL: https://omniweb.gsfc.nasa.gov/html/ow_data.html (accessed July 5, 2024).

URL: https://wdc.kugi.kyoto-u.ac.jp/wdc/Sec3.html (accessed July 5, 2024).

Original Russian version: Karakhanyan A.A., Molodykh S.I., published in Solnechno-zemnaya fizika. 2025, vol. 11, no. 1, pp. 55–62. DOI: 10.12737/szf-111202506. © 2024 INFRA-M Academic Publishing House (Nauchno-Izdatelskii Tsentr INFRA-M)

How to cite this article

Karakhanyan A.A., Molodykh S.I. Tropospheric response to solar effects during geomagnetic superstorms in solar cycle 23. *Solar-Terrestrial Physics*. 2025, vol. 11, no. 1, pp. 49–55. DOI: 10.12737/stp-111202506.